Defense Threat Reduction Agency
8725 John J. Kingman Road, MS 6201
Fort Belvoir, VA 22060-6201

DTRA-TR-14-7

TECHNICAL REPORT

Photonic-Networks-on-Chip for High Performance Radiation Survivable Multi-Core Processor Systems

Approved for public release, distribution is unlimited.

December 2013

HDTRA1-03-D-0009

Prof. Luke F. Lester and Prof. Ganesh Balakrishnan

Prepared by:
OVPR/University Strategic Partnership
MSC02 1660
1 University of New Mexico
Albuquerque, NM 87131

DESTRUCTION NOTICE:

Destroy this report when it is no longer needed.
Do not return to sender.

PLEASE NOTIFY THE DEFENSE THREAT REDUCTION AGENCY, ATTN: DTRIAC/ J9STT, 8725 JOHN J. KINGMAN ROAD, MS-6201, FT BELVOIR, VA 22060-6201, IF YOUR ADDRESS IS INCORRECT, IF YOU WISH THAT IT BE DELETED FROM THE DISTRIBUTION LIST, OR IF THE ADDRESSEE IS NO LONGER EMPLOYED BY YOUR ORGANIZATION.

REPORT DOCUMENTATION PAGE

Form Approved
OMB No. 0704-0188

Public reporting burden for this collection of information is estimated to average 1 hour per response, including the time for reviewing instructions, searching existing data sources, gathering and maintaining the data needed, and completing and reviewing this collection of information. Send comments regarding this burden estimate or any other aspect of this collection of information, including suggestions for reducing this burden to Department of Defense, Washington Headquarters Services, Directorate for Information Operations and Reports (0704-0188), 1215 Jefferson Davis Highway, Suite 1204, Arlington, VA 22202-4302. Respondents should be aware that notwithstanding any other provision of law, no person shall be subject to any penalty for failing to comply with a collection of information if it does not display a currently valid OMB control number. **PLEASE DO NOT RETURN YOUR FORM TO THE ABOVE ADDRESS.**

1. REPORT DATE *(DD-MM-YYYY)*	**2. REPORT TYPE**	**3. DATES COVERED** *(From - To)*
00-12-2013	Technical	07/21/2010 - 04/30/2012

4. TITLE AND SUBTITLE

Photonic-Networks-on-Chip for High Performance Radiation Survivable Multi-Core Processor Systems

5a. CONTRACT NUMBER
DTRA01-03-D-0026

5b. GRANT NUMBER

5c. PROGRAM ELEMENT NUMBER

6. AUTHOR(S)

Prof. Luke Lester and Prof. Ganesh Balakrisnan

5d. PROJECT NUMBER
4

5e. TASK NUMBER
26

5f. WORK UNIT NUMBER

7. PERFORMING ORGANIZATION NAME(S) AND ADDRESS(ES)

OVPR/University Strategic Partnership
MSC02 1660
1 University of New Mexico
Albuquerque, NM 87131

UNM Center for high technology Materials
MSC 04-2710
1313 Goddard SE
Albuquerque, NM 87106

8. PERFORMING ORGANIZATION REPORT NUMBER

9. SPONSORING / MONITORING AGENCY NAME(S) AND ADDRESS(ES)

Defense Threat Reduction Agency
8725 John J. Kingman Road STOP 6201
Fort Belvoir, VA 22060
PM/James Reed

10. SPONSOR/MONITOR'S ACRONYM(S)
DTRA

11. SPONSOR/MONITOR'S REPORT NUMBER(S)
DTRA-TR-14-7

12. DISTRIBUTION / AVAILABILITY STATEMENT

Approved for public release; distribution is unlimited.

13. SUPPLEMENTARY NOTES

14. ABSTRACT

The University of New Mexico has undertaken a study to determine the effects of radiation on Quantum Dot Photonic Integrated Circuits (QDPICs). Over the course of the last year, the constituent III-V active semiconductor materials and Si-photonic components forming these QDPICs have been designed, grown and fabricated. Photoluminescence studies before and after radiation exposure have been conducted on bare wafer samples for the III-V quantum-confined laser materials to isolate the damage to the active semiconductor materials themselves. Further techniques to probe radiation damage at the wafer level have been highlighted as well as methods to assess performance degradation at the device level. These studies should pave the way towards the quantitative assessment of the survivability of next-generation multi-cell processors based on optical interconnects.

15. SUBJECT TERMS

Radiation resistant materials, Quantum Dot Photonic Integrated Circuits, Si-photonics, quantum dot lasers, mode-locked lasers

16. SECURITY CLASSIFICATION OF:			**17. LIMITATION OF ABSTRACT**	**18. NUMBER OF PAGES**	**19a. NAME OF RESPONSIBLE PERSON**
a. REPORT	**b. ABSTRACT**	**c. THIS PAGE**	UU	20	James Reed
Unclassified	Unclassified	Unclassified			**19b. TELEPHONE NUMBER** *(include area code)* 703-767-8793

CONVERSION TABLE

Conversion Factors for U.S. Customary to metric (SI) units of measurement.

MULTIPLY →	BY →	TO GET
TO GET ←	BY ←	DIVIDE
angstrom	1.000 000 x E -10	meters (m)
atmosphere (normal)	1.013 25 x E +2	kilo pascal (kPa)
bar	1.000 000 x E +2	kilo pascal (kPa)
barn	1.000 000 x E -28	meter^2 (m^2)
British thermal unit (thermochemical)	1.054 350 x E +3	joule (J)
calorie (thermochemical)	4.184 000	joule (J)
cal (thermochemical/cm^2)	4.184 000 x E -2	mega joule/m^2 (MJ/m^2)
curie	3.700 000 x E +1	*giga bacquerel (GBq)
degree (angle)	1.745 329 x E -2	radian (rad)
degree Fahrenheit	$t_k = (t^\circ f + 459.67)/1.8$	degree kelvin (K)
electron volt	1.602 19 x E -19	joule (J)
erg	1.000 000 x E -7	joule (J)
erg/second	1.000 000 x E -7	watt (W)
foot	3.048 000 x E -1	meter (m)
foot-pound-force	1.355 818	joule (J)
gallon (U.S. liquid)	3.785 412 x E -3	meter^3 (m^3)
inch	2.540 000 x E -2	meter (m)
jerk	1.000 000 x E +9	joule (J)
joule/kilogram (J/kg) radiation dose absorbed	1.000 000	Gray (Gy)
kilotons	4.183	terajoules
kip (1000 lbf)	4.448 222 x E +3	newton (N)
kip/inch^2 (ksi)	6.894 757 x E +3	kilo pascal (kPa)
ktap	1.000 000 x E +2	newton-second/m^2 ($N-s/m^2$)
micron	1.000 000 x E -6	meter (m)
mil	2.540 000 x E -5	meter (m)
mile (international)	1.609 344 x E +3	meter (m)
ounce	2.834 952 x E -2	kilogram (kg)
pound-force (lbs avoirdupois)	4.448 222	newton (N)
pound-force inch	1.129 848 x E -1	newton-meter (N-m)
pound-force/inch	1.751 268 x E +2	newton/meter (N/m)
pound-force/foot^2	4.788 026 x E -2	kilo pascal (kPa)
pound-force/inch^2 (psi)	6.894 757	kilo pascal (kPa)
pound-mass (lbm avoirdupois)	4.535 924 x E -1	kilogram (kg)
pound-mass-foot^2 (moment of inertia)	4.214 011 x E -2	kilogram-meter^2 ($kg-m^2$)
pound-mass/foot^3	1.601 846 x E +1	kilogram-meter^3 (kg/m^3)
rad (radiation dose absorbed)	1.000 000 x E -2	**Gray (Gy)
roentgen	2.579 760 x E -4	coulomb/kilogram (C/kg)
shake	1.000 000 x E -8	second (s)
slug	1.459 390 x E +1	kilogram (kg)
torr (mm Hg, 0^0 C)	1.333 22 x E -1	kilo pascal (kPa)

*The bacquerel (Bq) is the SI unit of radioactivity; 1 Bq = 1 event/s.

**The Gray (GY) is the SI unit of absorbed radiation.

Final Performance Report
Grant DTRA01-03-D-0009-0026

07/21/2010 - 4/30/2012

Prof. Luke F. Lester, Prof. Ganesh Balakrishnan
May 9, 2012

Abstract

The University of New Mexico has undertaken a study to determine the effects of radiation on Quantum Dot Photonic Integrated Circuits (QDPICs). Over the course of the last year, the constituent III-V active semiconductor materials and Si-photonic components forming these QDPICs have been designed, grown and fabricated. Photoluminescence studies before and after radiation exposure have been conducted on bare wafer samples for the III-V quantum-confined laser materials to isolate the damage to the active semiconductor materials themselves. Further techniques to probe radiation damage at the wafer level have been highlighted as well as methods to assess performance degradation at the device level. These studies should pave the way towards the quantitative assessment of the survivability of next-generation multi-cell processors based on optical interconnects.

Executive Summary

The aim of this project was to conduct a study of the degradation of quantum dot photonic integrated circuits (QDPICs) and their constituent components resulting from radiation exposure. Our initial investigations focused on basic radiation hardness assessments of the underlying semiconductor materials; namely the InAs quantum

dots (QDs) or quantum dashes (QDashes) making up the active regions of the III-V lasers at the heart of the photonic circuits. To date, our key initiatives have included the identification and growth of epitaxial designs that minimize radiation damage effects, in particular, in QD ensembles; irradiation of these samples with three distinct radiation sources; Design of QD mode-locked laser (MLLs) modules; highlighting the suitability of high-resolution cross-sectional scanning tunneling microscopy (STM) to image radiation-induced structural damage to the fabrication III-V nanostructures; and demonstrating the potential of the segmented contact method to characterize modal gain and loss in our QD MLLs and use these fundamental properties to assess changes in device performance. This work has resulted in the graduation of Dr. Chang-Yi Lin, in the Spring of 2011, who is currently employed at Intel-Hillsboro. His dissertation Title was "Microwave Techniques and Applications of Semiconductor Quantum Dot Mode-Locked Lasers". This can be found at the following web address:(**http://www.chtm.unm.edu/lester/Theses/CYLin_dissertation_final1.pdf**). The work also resulted in the following conference papers: R. Raghunathan, M. T. Crowley, F. Grillot, V. Kovanis and L. F. Lester, "Direct Characterization of Carrier Relaxation in a Passively Mode-Locked Quantum Dot Laser", Proceedings of IEEE Photonics Conference, pp 109-110, (2011) and Ravi Raghunathan, Mark T. Crowley, Frédéric Grillot, Sayan D. Mukherjee, Nicholas G. Usechak, Vassilios Kovanis, Luke F. Lester, "Delay Differential Equation-Based Modeling of Passively Mode-Locked Quantum Dot Lasers Using Measured Gain and Loss Spectra" Proceedings of SPIE **8255**, (2012) and in a journal publication: M. T. Crowley, D. Murrell, N. Patel, M. Breivik, C.-Y. Lin, Y. Li, B.-O. Fimland and L. F. Lester,"Analytical Modeling of the Temperature Performance of Monolithic Passively Mode-Locked Quantum Dot Lasers" IEEE J. Quantum Electron. **18**, 1059, (2011). And also an invited talk, "Optical Interconnects for Chip-to-Chip Communications" at Intel College of Engineering in June of 2011.

Research team: The following personnel have been engaged in this work: Prof. Luke Lester, Prof. Ganesh Balakrishnan, Dr. Mark Crowley and PhD candidates David Murrell and Pankaj Ahirwar.

Component design and fabrication

Growth of III-V semiconductor PL structures including InGaAs quantum well active regions on GaAs, InAs quantum dots-in-a-well (DWELL) structures where InAs dots are embedded in InGaAs quantum wells, and InAs quantum dashes grown on InP substrate and embedded in quartenary AlGaInAs quantum wells as well as GaSb dots grown on GaAs substrate, Si-photonic components, specifically, Si-photonic-based waveguides disc resonators and optical time division multiplexing devices were also designed and fabricated. The growth of the PL structures was carried out at UNM's state of art molecular beam epitaxy reactor facility. In particular the study of the DWELL structures has been most pertinent in our efforts to date. Details of their fabrication are presented below.

Multi-layer DWELL laser structure

The multi-layer DWELL laser structure is grown by molecular beam epitaxy (MBE) and consists of several stacks of dots in the active region. The layers are composed of an n-type (10^{18} cm^{-3}) 300-nm-thick GaAs buffer, an n-type lower $Al_xGa_{1-x}As$ (x=0.2) cladding layer, a GaAs core waveguide, a p-type upper cladding layer, and

a p-doped (3×10^{19} cm^{-3}) 60-nm-thick GaAs cap. The cladding layers are doped at 10^{17} cm^{-3} and are each 2-μm thick. In the center of the waveguide, up to 8 DWELL layers with 29 nm GaAs barriers are grown. QDs formed from about 2 monolayers of InAs are confined in the middle of a 10 nm thick $In_{0.15}Ga_{0.85}As$ QW in each layer. The QDs and QW were typically grown at 500 °C, as measured by an optical pyrometer. The QDs formed under these conditions have an areal density of about 3×10^{10} cm^{-2}, a base diameter <40nm, and are 7 nm high. Detailed descriptions of the DWELL growth technique can be found elsewhere [1, 2].

Devices are fabricated according to standard multi-section device processing [3]. After the first lithography with the ridge-waveguide-mask, the sample is etched to form 3-μm wide, 1.8-μm deep ridges by inductively coupled plasma (ICP) etching in BCl_3. Then a BCB layer is applied for isolation between the p-type metal and the etched cladding layer. The two-section contact mask is used to make photoresist patterns for the p-type metal deposition and ion implantation. After depositing Ti/Pt/Au to form the p-metal contact, an isolation between the adjacent sections is provided by proton implantation, with an isolation resistance of >10 MΩ. After the substrate had been thinned and polished, a Au/Ge/Ni/Au n-metal contact was deposited on the backside of the n^+-GaAs substrate and annealed at 380°C for 1 minute to form the n-ohmic contact. A temperature greater than 380°C can crack the BCB. Another Ti/Au metal layer was deposited for n-side mounting, and then the sample is cleaved to form devices with a short absorber section and long gain section. Typically, the InAs DWELL MLL has a ~1-mm absorber section and a ~7-mm gain section depending on the pulse repetition rate desired. The cleaved facet near the absorber section is HR-coated (R≈95%) to create self-colliding pulse effects in the saturable absorber for pulse narrowing. The other facet is low reflection (LR)-coated (R≈15%).

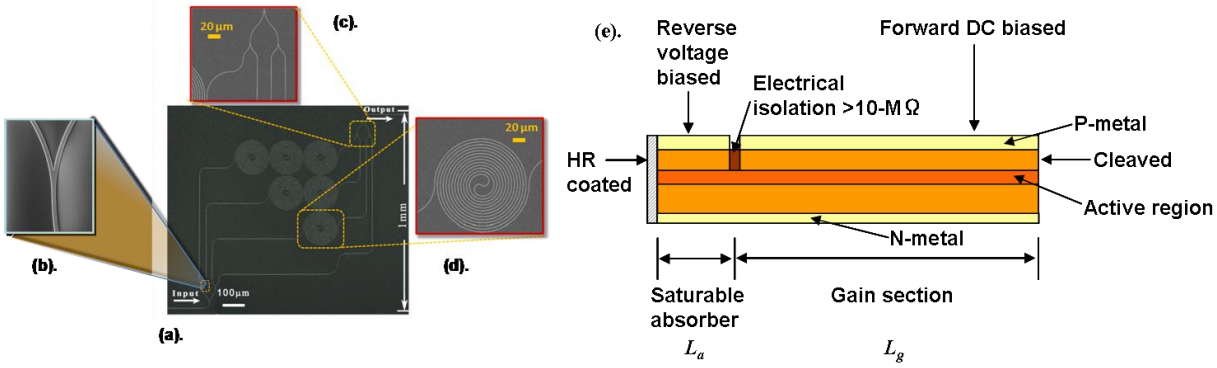

Fig. 1 Top view SEM of (a) the Si OTDM device and zoomed view of the (b) Y-splitter , (c) MUX, and (d) optical delay. (e) Shows a side view schematic of the two-section passively mode-locked quantum dot laser.

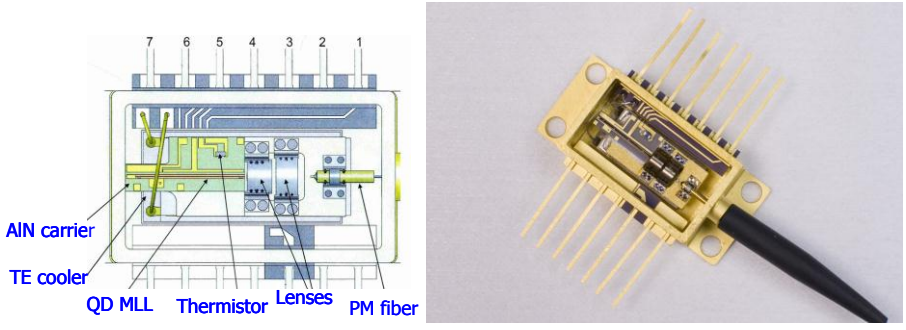

Fig. 2 (a) Design layout of fully packaged QD MLL complete with temperature control, optical lenses and polarization maintaining fiber pigtail. (b) Photograph of the packaged QD MLL module with top casing removed. Photos and devices courtesy of Innolume, Inc.

Irradiation sources and studies

For our initial radiation hardness assessments we subjected sections of the bare quantum dot material wafers to ^{137}Cs radiation and compared this to a control wafer of the same material. Our procedure of investigation examines the Photoluminescence (PL) changes as the sample goes through irradiation sessions. The ^{137}Cs source delivered radiation with 0.605 Mev and the material experienced a total radiation dose of 311 kRad. Care was taken to ensure that the PL measurement setup is calibrated consistently across each measurement run by using a control sample before the test sample is measured. To determine the impact of radiation exposure on the dot sample we measured PL before and after irradiation. Analysis of the PL peak's full width half max, peak height, and integrated intensity provide the points of comparison to determine the extent of damage incurred through illumination runs.

PL Setup

The PL measurement setup that we use is shown schematically in figure 3. The light source is an electrically pumped HeNe laser operating at the fundamental lasing wavelength of 632.8 nm at a power of less than 5 W. This power is sufficient to excite PL in the sample which has a bandgap in the 1.3-μm range.

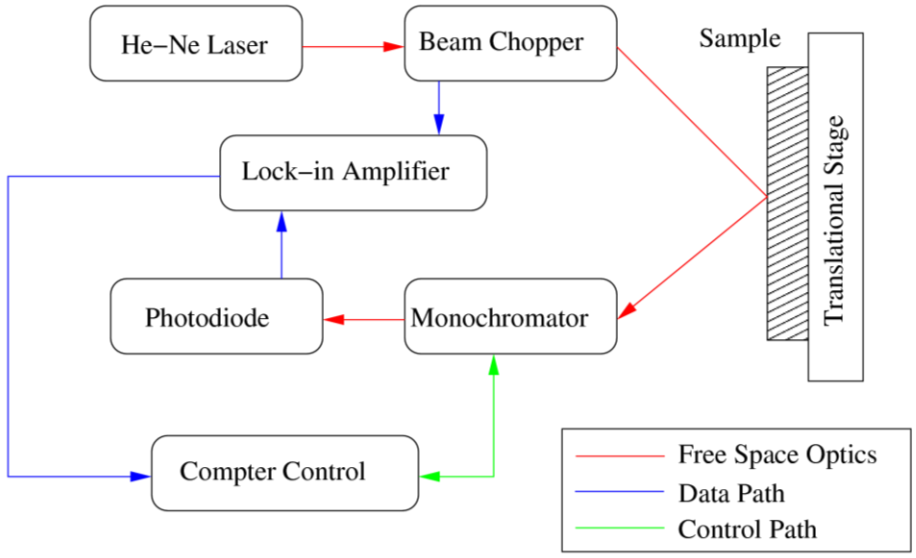

Fig. 3 Schematic of photoluminescence (PL) measurement setup.

Background light is eliminated through the use of a lock-in amplifier synchronized to a rotating beam chopper at the laser facet. A band pass filter restricts the linewidth of the HeNe to its fundamental line only. Collected PL light is separated from the exciting beam through the use of another filter (not shown in figure 3) before passing through a monochromator. The monochromator is computer controlled allowing for stepped scans of the PL spectrum using the attached photodiode detector. Data is collected after the lock-in amplifier has integrated out the noise of the signal caused by background light.

Initial irradiation studies: Effect on material PL

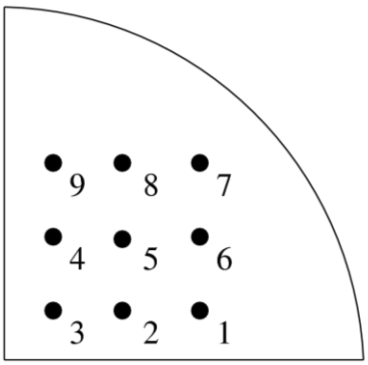

Fig. 4 Illustration of the positions on the wafer where the photoluminescence measurements are performed. The measured photoluminescence at these positions is presented in fig. 5.

Initially, measurement of the InAs DWELL quantum dot gain media involved examination of quarter sections of a single 2-inch wafer. The quantum dot material consisted of 3 stacks of InAs dots-in-a-well type structure. Measurement points were defined relative to the inner corner of the wafer as shown in figure 4. These points were probed and positioned using the micrometers on the translation stage. Typical PL measurements are shown in figure 5. The first observation one can make from this data is that the dot concentration and properties are not uniform across the entire surface of the wafer segment as a result of the growing process by MBE. Because of the slight asymmetry in the growth process requires precise sampling of each point before and after irradiation. This initial run did not yield any significant change in the PL spectra both immediately after exposure and several days afterwards. Problems in making consistent measurements at each of the prescribed points in figure 4 motivated a change in the test sample geometry. Cleaving a rectangular bar from the wafer as opposed to the full quarter wafer allowed us to make more consistent measurements by reducing the area of the sample, allowing for us to profile the PL intensity in a more seamless way. It became clear immediately after our first irradiation run that the lower energy of the ^{137}Cs source was insufficient to cause damage in a reasonable testing time period. Thus, we gained access to a linear accelerator that could produce photon streams of high energy and intensity. We irradiated the sample with 15 MeV photons for a brief period of time such that the sample accumulated a total dose of ~13kRad. PL measurements of the wafer bar were taken before and after the irradiation session. The full width half max of the sample's PL peak is shown in fig. 6 and the change in max intensity is presented in fig. 7. The distance on the x-axis of both plots represents the distance from a reference point proceeding outwards from the original wafer center. The results in both figs. 6 and 7 indicate that despite exposure to a higher energy radiation source the degradation of the measured QD material PL characteristics is negligible.

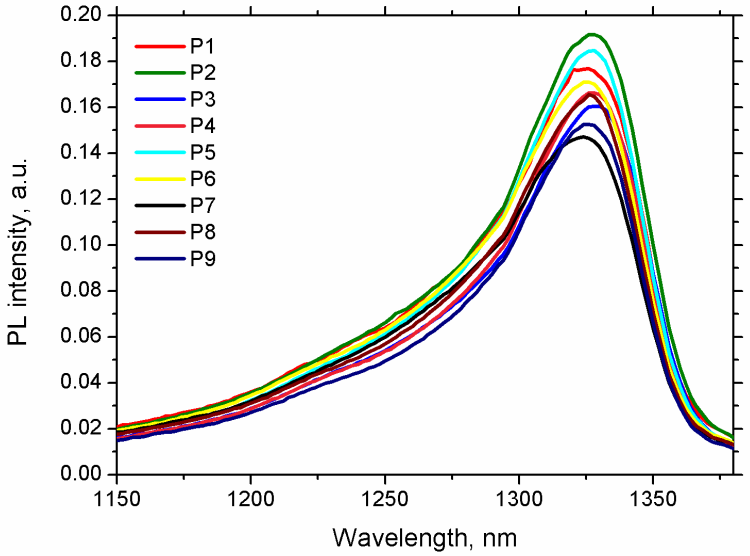

Fig. 5 Measured photoluminescence at various positions on the quantum dot wafer. The positions on the wafer where the photoluminescence is measured are described in fig. 4.

Overall, it was concluded that the radiation sources used in our initial studies did not demonstrate a large enough radiation flux to damage the quantum dot material under investigation. In response, a new collaboration with the Air Force Research Laboratory at Kirtland Air Force base was established in order to gain access a more intense, ^{60}Co, radioactive source.

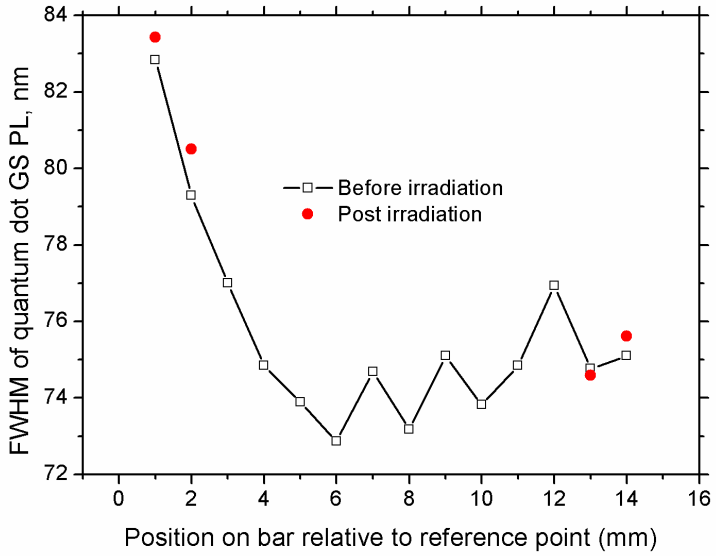

Fig. 6 Measured photoluminescence FWHM (~1325 nm) measured at various positions on the "bar" cleaved from the quarter segment of the quantum dot wafer sample. The reference point was the original wafer center.

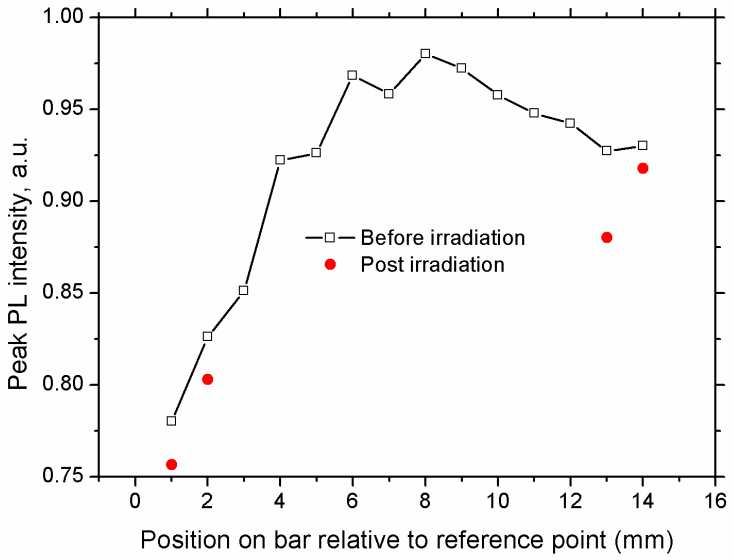

Fig. 7 Measured peak photoluminescence measured at various positions on the "bar" cleaved from the quarter segment of the quantum dot wafer sample. The reference point was the original wafer center.

This source allowed for exposures ranging from 1-2 MRad. However, despite turning to more active radioactive sources, it was established ultimately that the PL technique used to characterize the post irradiation damage was inadequate. As a consequence, our final efforts were directed at highlighting suitable techniques to characterize changes in the materials both at the wafer and device level.

Cross-sectional scanning tunnelling microscopy

During the course of this program we have investigated cross-sectional scanning tunneling microscopy (STM) as a technique that can be used for the investigation of ionizing radiation damage to quantum dot structures. The investigation consisted of the growth of various quantum dot structures which were then investigated with cross sectional STM. There were two material systems that were investigated. The first was a classic InAs Quantum dot structure in a GaAs matrix and the second material was GaSb quantum dots in a GaAs matrix. The samples were grown at the Center for High Technology Materials and subsequently send to TU Berlin for investigation using their cross-section STM facilities.

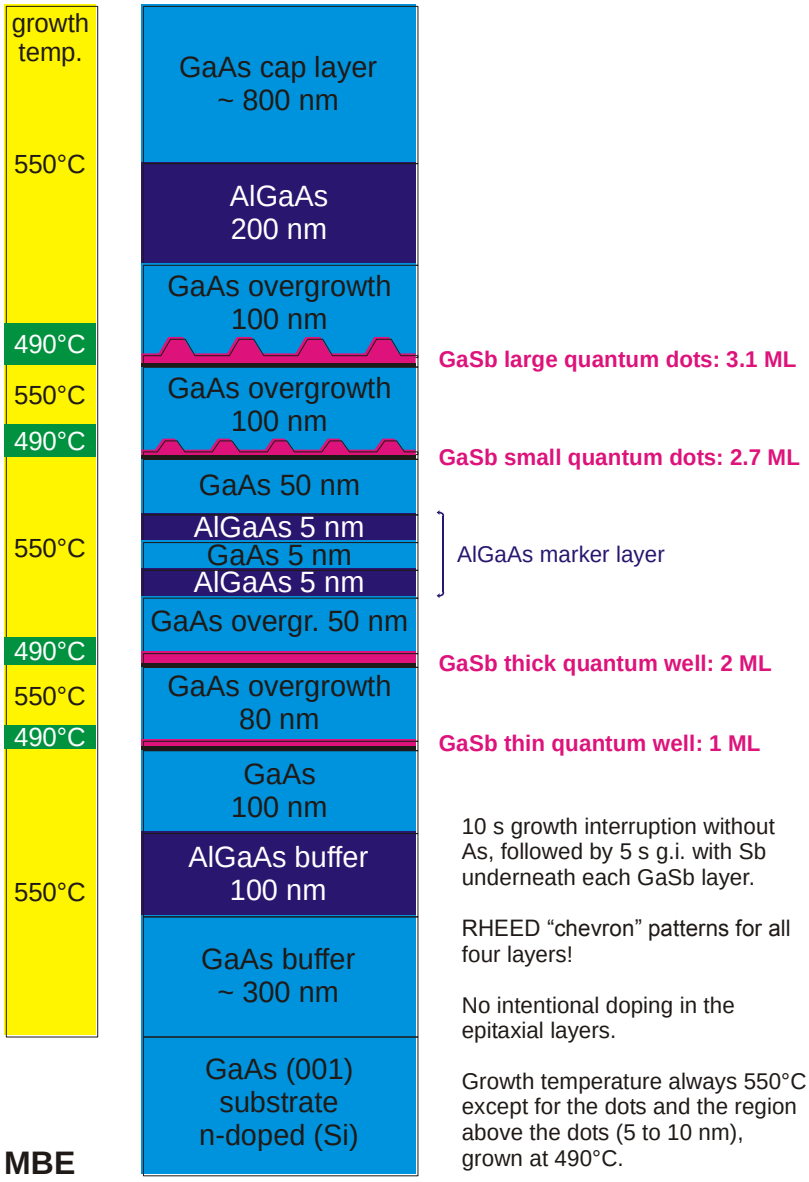

Fig.8: Schematic of the growth structure for the GaSb/GaAs quantum dots.

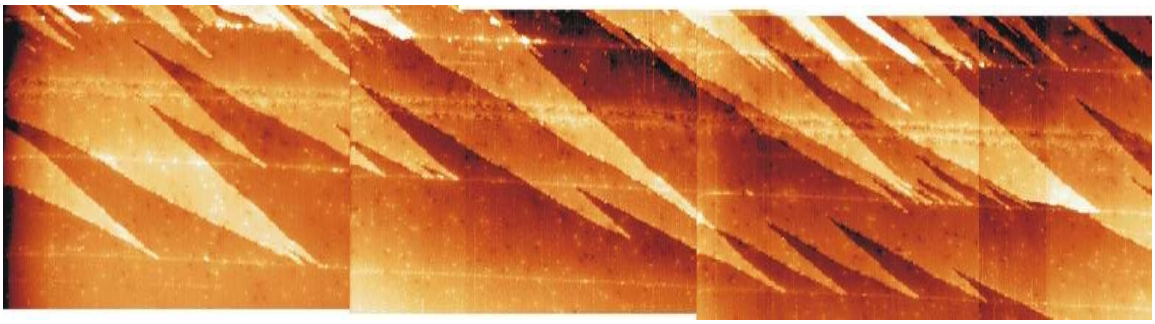

Fig.9: In-situ cleaved sample with the dot layers visible in low resolution.

The typical growth structure for both the InAs and the GaSb quantum dots is shown in figure 8. The structure typically consists of multiple dot layers with different dot material coverage which are then spaced widely apart from each other. The logic behind the approach is to be able to decouple the strain field from one dot layer to the other while also being able to allow for irradiation studies where the damage from dot to dot as a function of thickness and areal dot density can be measured.

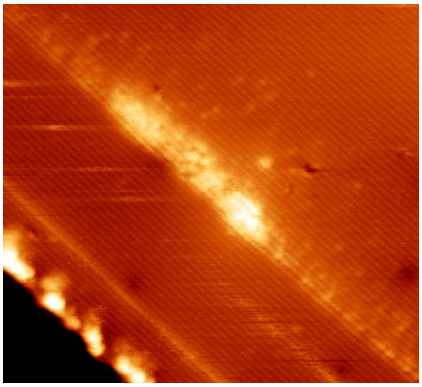

Fig.10: High resolution cross-sectional STM image of GaSb quantum dot.

Prior to conducting the cross-sectional STM we have performed a variety of experiments on the dots such as atomic force microscopy, transmission electron microscopy and photoluminescence studies. These studies are done to ensure that the samples are carefully characterized prior to irradiation. The samples are then measured post irradiation. The irradiated and characterized samples are then shipped to the STM laboratory. The process of STM is done with the sample clamped in a vacuum chamber and an in-situ cleaving apparatus is used for cleaving the sample. This results in a pristine cleave with no native oxide on the surface. This is a very critical step in achieving atomic resolution and by definition a surface optimal for conducting radiation damage studies. Figure 10 presents a high resolution cross-sectional STM image of a GaSb/GaSb quantum pre-irradiation. The GaSb itself appears as a bright structure in the center of the image. The extent to which this characterization work has been completed includes the growth of a library of samples consisting of GaSb and InAs quantum dots and the subsequent characterization and cross-sectional STM of the samples. Further studies in this process would include a similar study of the same samples that have been irradiated. The imaging of the surface under a variety of biases would result in the highlighting of defects in the materials from the process of ionizing damage. This would then allow us to understand the extent of the damage to the dots and how this damage can be localized to a few dots so as to make the device radiation hardened.

Quantum dot gain and absorption measurements

This section details an approach used to quantify the changes in nanostructure gain and absorption as a function of a given external physical parameter such as radiation dosage or temperature. To illustrate the viability of the approach we validate its accuracy for broad variations in ambient temperature. The effect of temperature on the gain and loss characteristics of the underlying nanostructure gain material and also how this effects the performance of monolithic two-section passively mode-locked lasers based on the same nanostructure active region is investigated. A set of equations based on an analytic net-gain modulation phasor approach is used to model the observed mode-locking stability of these devices over temperature. The equations used rely solely on static material parameters, measured on the actual device itself, namely, the modal gain and loss characteristics, and govern the limit describing the onset of mode-locking. Employment of the measured gain and loss characteristics of the gain material over temperature, wavelength and current injection in the model provides a physical insight as to why the mode-locking shuts down at elevated temperatures. The model enables a temperature-dependent prediction of the range of cavity geometries (absorber to gain length ratios) where mode-locking can be maintained. Excellent agreement between the measured and the modeled mode-locking stability over a wide temperature range is achieved for an 8-stack InAs/GaAs quantum dot mode-locked laser. Similarly, this approach can be used where radiation dosage is the external physical parameter that is varied. This is an attractive tool to guide the design of monolithic passively mode-locked lasers for applications where the device will be subjected to and be expected to operate in an environment with wide variations in certain external physical parameters.

The multi-section QD laser was mounted on a copper heatsink and the measurements were performed at controlled substrate temperatures ranging from 20 °C to 70 °C using a Peltier-based element to stabilize the temperature. The segmented contact method was used to characterize the modal gain and loss characteristics of the active region material system. This approach is particularly suited to low dimensional semiconductor gain media such as those composed of QDs and quantum dashes where the magnitude of the internal loss can be of the same order as the net modal gain. Further details pertaining to this measurement technique, including the experimental set-up, can be found in Xin *et al* [3]. Figures 11, 12 and 13 present the measured modal gain and total loss characteristics of the QD material. In these measurements, the current density applied to the gain section is limited to 1.6 kA/cm^2 to avoid potential damage to the device. The reverse bias on the saturable absorber section is varied from 0 to 5 V. Figures 3 and 4 show the measured total loss spectra over temperature for reverse voltage values of 0 V, 1 V, 3 V and 5 V. The total loss evaluated at the gain peak for each temperature is indicated in Figs. 11 and 12 by the dashed lines. The internal loss can be extracted from the long wavelength side of the total loss spectra. An averaged value of 3.3 cm^{-1} is determined here for this device

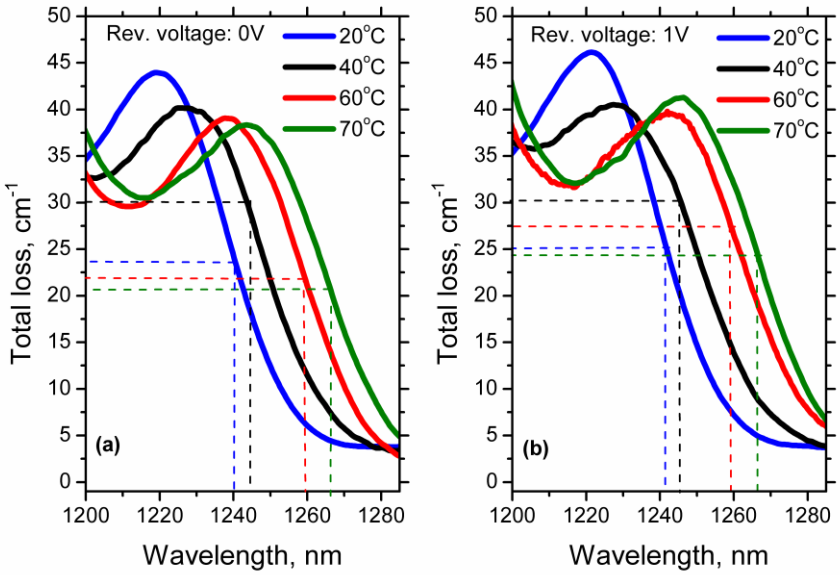

Fig. 11 Measured temperature-dependent total loss spectra at 0 V reverse bias (a) and 1 V reverse bias (b) measured on the multi-section device using the segmented contact method. The dashed lines guide the eye to the total loss values evaluated at the gain peak for each temperature considered. The unsaturated absorption, a_0, is acquired by subtracting the internal loss from the total loss.

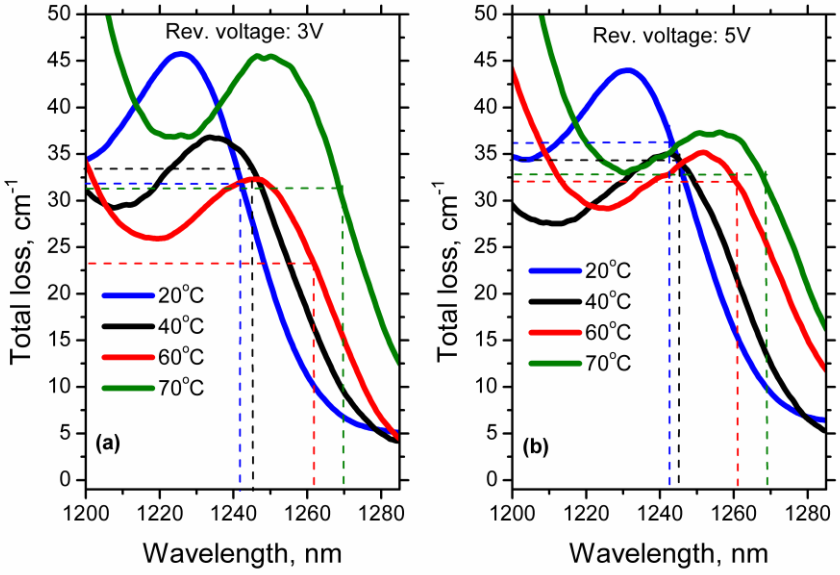

Fig. 12 Repeat of Fig. 11 for reverse voltages of 3V (a) and 5V (b).

over the temperature range considered. Figure 13 (a) shows the measured net modal gain spectra for a range of heat sink temperatures and a constant current density of 1.4 kA/cm^2. The gain is measured up to 70 °C where it was noted that the device continued to operate from the ground state QD transition. Two localized transitions are apparent in the spectra corresponding to the QD ground state (GS) and QD first excited state (ES), which appear at 1238 nm and 1174 nm at 20 ^{o}C, respectively (blue plot in Fig. 5 (a)).
The ground state gain magnitude is observed to decrease from 10.4 cm^{-1} to 7.0 cm^{-1} when the temperature increases from 20 ^{o}C to 70 ^{o}C, a 32% degradation. The ES degrades even more substantially from 13.6 cm^{-1} at 20 ^{o}C to 6.7 cm^{-1} at 70 ^{o}C, a 51% degradation.

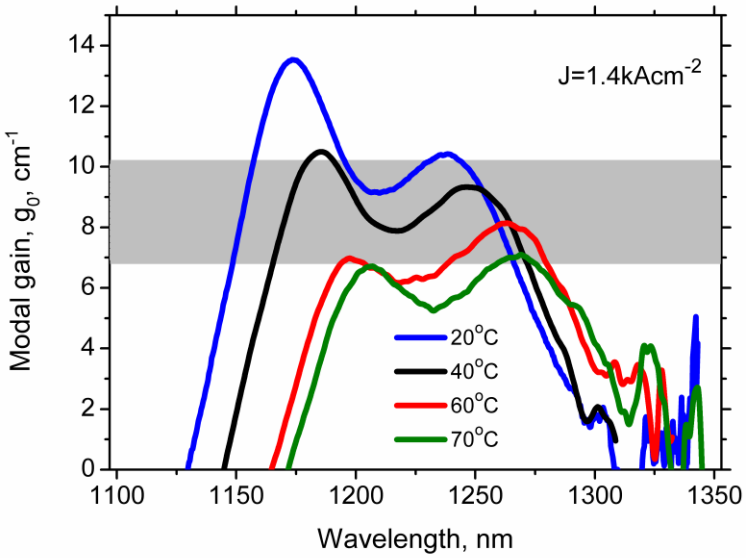

Fig. 13 (a) Measured modal gain spectra for a current density of 1.4 kA/cm^2 measured on the multi-section device using the segmented contact method for temperatures ranging from 20 ^{o}C to 70 ^{o}C. The ground state modal gain peak (~1240 nm at 20 ^{o}C (blue plot)) is observed to shift at a rate of 0.6 nm/ ^{o}C to 1268 nm at 70 ^{o}C (green plot) and reduce in magnitude from 10.4 cm^{-1} at 20 ^{o}C (blue plot) to 7.0 cm^{-1} at 70 ^{o}C (green plot). The gray band illustrates the range of threshold gain values covered in this study.

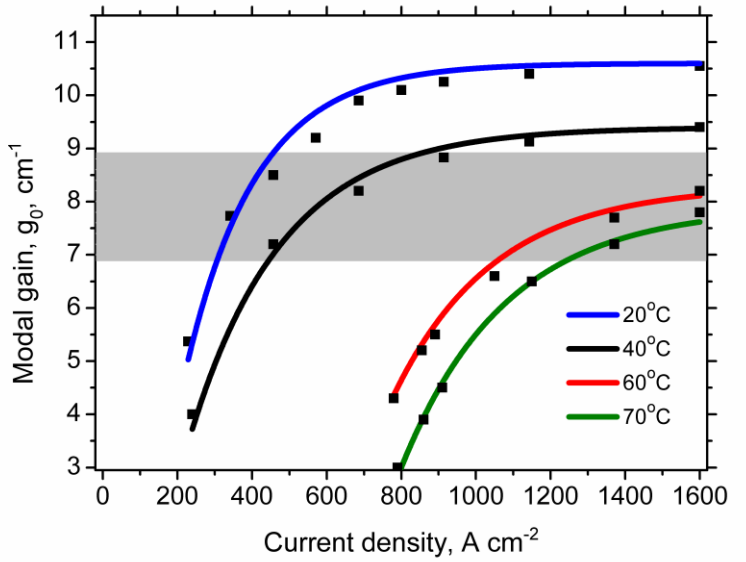

Fig. 13 (b) Measured modal gain (solid squares) as a function of current density measured on the multi-section device using the 3-section segmented contact method. The solid curves are the resulting fits using (3). For each temperature and current density the gain value is taken at the gain peak. The gray band illustrates the range of threshold gain values.

Analytic modeling of QD mode-locked lasers

The classic paper of Lau and Paslaski experimentally demonstrated that the onset of passive mode-locking in a semiconductor laser appears as a sinusoidal modulation of the optical intensity output of the laser [4]. Theoretically, they described this boundary using a net-gain modulation phasor approach and simultaneously derived expressions that ensured minimization of self-pulsation contamination. Our recent work extended the aforementioned formalism to account for the discrete distribution of the gain and saturable absorber sections in a laser cavity [5]. The following equation was derived in that study,

$$\frac{L_a}{L_g} > \left(\frac{\frac{dg_0}{dJ}}{\frac{dg_0}{dJ}\Big|_{g_0=0}} \right)^2 \frac{g_o}{a_o} \qquad (1)$$

where L_a and L_g are the length of the absorber and gain sections, respectively, g_0 and a_0 are the modal gain in the gain section and unsaturated absorption in the absorber region, respectively, dg_0/dJ is the differential gain, and the differential quantity in the denominator of (1) represents a conservative approximation for the differential absorption [5]. This extension enabled the prediction of functional device layouts using the measured gain and loss characteristics as input. The model has been employed for the cavity design of two-section passively mode-locked lasers based on several different material systems [6]. The method is based on the assumption that the net gain modulation (g_0-a_0) is sinusoidal and in phase with the photon density modulation. An additional constraint within the model comes in the form of the threshold condition for lasing:

$$\frac{L_a}{L_g} = \frac{g_0 - \alpha_m - \alpha_i}{a_0 + \alpha_m + \alpha_i} \qquad (2)$$

In (2) above, α_i is the internal loss, α_m is the mirror loss, while L_a and L_g are the lengths of the gain and absorber section of the two-section device respectively. From (1) and (2), it is readily apparent that in order to strengthen the mode-locking condition over temperature, one can, for instance, reduce the variation of the modal gain with temperature by engineering the gain material and reducing the internal losses. On the other hand, one can optimize the ratio L_a/L_g, the latter being the approach examined in this work. Equations (1) and (2) can be considered as describing the hard boundary defining the onset of mode-locking, the limiting case or minimum requirement. Although the model does not have the capability to predict the pulse duration since a sinusoid is assumed, it is nevertheless a useful tool to predict the onset of mode-locking over a broad temperature range.

Here we seek to provide a practical method which allows one to determine whether a given MLL can maintain mode-locking over a desired temperature range and if not, to understand why it fails. In comparison to our recent delay differential equation model [7] and the work of Vladimirov and Turaev [8], the advantage of this analytical approach is the ability to predict functional MLL device layouts through the use of measured temperature-dependent static laser parameters measured on the actual device under investigation. Consequently, valuable insight can be gained without knowing dynamic material parameters such as the carrier lifetime or the gain/absorption recovery times of the active semiconductor material.

Figure 14 (b)-(d) shows modeled mode-locking stability maps where the boundaries between hatched and white areas represent the extreme boundary for the onset of mode-locking. Stable mode-locking without self-pulsation is predicted to exist within the individual contours for each temperature considered [4]. The upper bound of each contour is determined by (2), whereas (1) describes the lower bound of these maps. Fig. 14 (b) displays one such set of contours when 0 V is applied to the saturable absorber as a function of the ratio L_a/L_g and the gain section threshold current density, J_{th}. The two-section passive QD MLL used to experimental verify these

predictions had an L_a/L_g ratio of 0.14, highlighted by the dashed black line in Figs. 14 (b)-(d). Mode-locking in the regions above the upper parts of the boundaries does not occur because the laser cannot operate given the magnitude of the losses present. Note that the gain per unit length is considerably less than the absorption per unit length, typically a factor of 5 difference, as shown in Tables I and II.

TABLE I

TABLE OF MEASURED (ON THE MULTI-SECTION DEVICE) TEMPERATURE-DEPENDENT LOSS CHARACTERISTICS FROM LEFT TO RIGHT: THE REVERSE BIAS ON THE SATURABLE ABSORBER, THE WAVELENGTH OF PEAK ABSORPTION, THE PEAK MAGNITUDE OF THE ABSORPTION (INCLUDES INTERNAL LOSS), AND THE UNSATURATED ABSORPTION (TAKEN AT THE GAIN PEAK AND ASSUMING AN AVERAGED INTERNAL LOSS OF 3.3 CM^{-1} OVER THE TEMPERATURE RANGE CONSIDERED).

Temp, (^oC)	Reverse bias, (V)	a_{peak}, (nm)	a_{max}, (cm^{-1})	a_0, (cm^{-1})
20	0	1219.2	44.6	20.
40	0	1227.6	41.1	26.2
60	0	1238.4	40.2	18.7
70	0	1244.4	39.8	17.7
20	1	1222.0	46.3	21.7
40	1	1228.4	40.8	28.7
60	1	1240.4	39.1	18.2
70	1	1245.0	41.4	19.7
20	3	1227.0	46.2	28.7
40	3	1235.0	37.2	31.2
60	3	1245.6	32.6	21.0
70	3	1249.6	45.8	29.7
20	5	1232.0	44.4	32.9
40	5	1242.0	35.5	31.5
60	5	1250.4	35.6	30.0
70	5	1254.0	37.5	29.7

TABLE II

TABLE OF MEASURED TEMPERATURE-DEPENDENT PARAMETERS FROM LEFT TO RIGHT: THRESHOLD CURRENT DENSITY OF THE TWO-SECTION DEVICE , PEAK GAIN WAVELENGTH AND MODAL GAIN VALUE MEASURED ON THE MULTI-SECTION DEVICE AT 1.6 KA/CM^2. NO LASING WAS OBSERVED AT 5 V AND 60 ^oC AND AT 70 ^oC FOR CURRENT DENSITIES UP TO 1.6 KA/CM^2.

Temp, (^oC)	J_{th} at 0V,1V,3V,5V, (A/cm^2)	G_{peak}, (nm)	g_0 at J=1.6kA/cm^2, (cm^{-1})
20	357, 387, 462, 537	1238	10.5
40	564, 616, 744, 811	1249	9.4
60	713, 792, 953 , no lasing	1261	8.3
70	No lasing	1268	7.7

One should realize that the tendency for the lower bounds of the maps to approach vanishingly small absorber lengths is an artifact of the gain saturation model used, (3), and arises from the gain saturating completely and consequently approaching a zero differential gain. However, in practice, the differential gain will never be zero due to the existence of excited dot states as well as the higher energy states surrounding the dots. Including this mechanism in (3) would ensure that the differential gain could never reach zero. However, there is some physical meaning to the absorber length becoming very small. In that case, the laser will switch to excited state operation. This behavior has been observed elsewhere [24]. The modeled maps displayed in Fig. 6 (a)-(d) predict stable mode-locking at 20 °C and 40 °C for the full range of absorber reverse bias values considered (0 V-5 V). The upper bounds of the maps follow the saturation of $g_0(J)$. The model also predicts that the device will not mode-lock at 70 °C and that mode-locking will shut down at 60 °C for absorber bias values greater than 3 V (examine Fig. 6 (c) and (d)). Physically, this occurs because the available gain cannot overcome the cavity losses. In contrast to the 20-40°C, predictions, the fact that the measured threshold current at 60°C (open red symbol in Fig. 6) does not fall within the boundary of the 60°C contour (red plot) is a tell-tale sign that the mode-locking will not be as stable as that observed at cooler temperatures. The underlying physical reasons for this behavior will be discussed in more detail in section VI in terms of the measured gain and loss presented in Tables I and II.

With increasing temperature the contours in Fig. 6 close up and shift towards lower L_a/L_g ratios as a result of the degradation in g_0, see Fig. 5. The plots in Fig. 6 predict that there exists a range of cavity layouts that permit mode- locking over the 20-70°C temperature range investigated. In fact, Fig. 6 is pointing towards shorter absorber sections to compensate for the temperature mediated deterioration of g_0 in order to permit broader temperature insensitivity. For example, an L_a/L_g ratio of 0.075 (Fig. 6) is predicted to ensure mode- locking from 20 °C to 70 °C and 0-5 V.

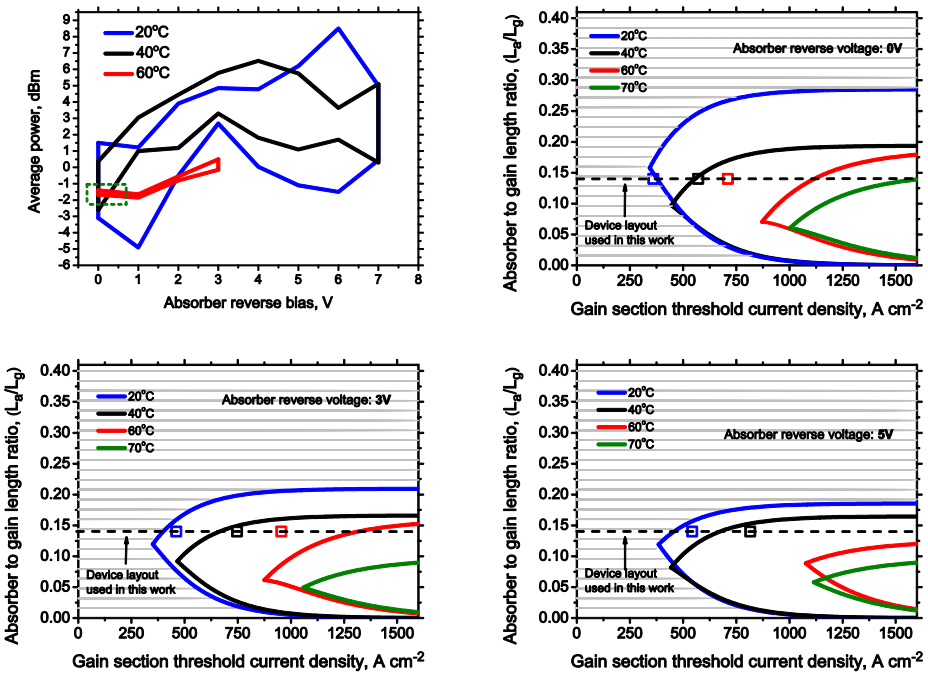

Fig. 14 (a) Measured mode-locking (ML) stability maps and (b)-(d): Modeled ML stability maps corresponding to an absorber reverse bias of 0V, 3V and 5V in (a). The dashed black line is a guide for the eye illustrating the absorber to gain length ratio of the two-section QD MLL characterized in this work with a 1-mm absorber section and a 7-mm gain section. The hatched region indicates the geometries and gain section current densities where ML cannot be achieved for this material. The maps define the hard boundary for the onset of ML. In agreement with the measurements in (a) the model predicts that although ML at 70 ^{o}C is not possible for the two-section cavity geometry of the device used in this work, ML is possible for shorter absorber section to gain section length (L_a/L_g) ratios.

To substantiate the predictions of the model in the previous section, this section concentrates on measuring

the impact of temperature on the mode-locking stability of the two-section passively mode-locked QD laser fabricated from the same material used in the gain and loss characterization. An RF spectral analysis and an autocorrelator are relied upon to characterize the mode-locking. Specifically, we identify stable mode-locking when at least two harmonics with 15-20 dB extinction ratio are obtained from the RF spectrum analyzer. The pulse-width was retrieved from autocorrelation measurements assuming a Gaussian pulse shape. The measured ability of the device to mode-lock over temperature for a range of absorber reverse bias values is presented in Fig. 14 (a).

To facilitate a comparison to the modeling presented in the previous section, the maps in Fig. 14 (a) define the pulse width observed before the mode-locking broke down. Typically, this is observed to occur for pulse widths in the range 15 ps (ML stability rapidly degrades for durations greater than these values). These pulse width trends are observed consistently over the entire temperature range considered. In fact, this is the shortest pulse width at 60 °C for absorber reverse bias voltages between 0 V and 3 V, resulting in the thin contour (red plot in Fig. 14 (a)). Thus this can be considered a reasonable assumption to the sinusoidal modulation for which the modeling of the previous section is based. In comparing the modeled and measured ML maps, it should be stressed that the model does not predict pulse widths but rather gives an indication of whether mode-locking is likely to be achieved or not.

Between 20 °C and 40 °C, the device exhibits stable mode-locking over a wide range of operating conditions, however, the performance at 60 °C deteriorates dramatically and mode-locking was not observed beyond 3 V absorber reverse bias at this temperature, see Fig. 14 (a). The device did not mode-lock at 70 °C for the range of current densities used. The tendency, at elevated temperature, for the device not to mode-lock at higher absorber reverse voltages (Compare 60 °C (red contour) and 20 °C (black contour) maps in Fig. 14 (a)) has been reported previously [9, 10] and is attributed to the increasing sweep out of carriers from the saturable absorber as the temperature increases. The calculated and measured ML stability match closely, highlighting the accuracy and effectiveness of the approach. The approach presented here should not only motivate the design of more temperature resistant gain media but should also effectively guide the optimization of current QD technologies in terms of p-doping and number of stacked QD layers. Indeed, it should prove to be an invaluable tool for the design of next generation devices capable of operation over broad temperature excursions.

References

[1] Liu, G. T., Stintz, A., Li, H., Malloy, K. J., and Lester, L. F., "Extremely low room-temperature threshold current density diode lasers using InAs dots in In0.15Ga0.85As quantum well," Electronics Letters **35**(14), 1163-1165 (1999).

[2] Stintz, A., Liu, G. T., Gray, A. L., Spillers, R., Delgado, S. M., and Malloy, K. J., "Characterization of InAs quantum dots in strained InxGa1-xAs quantum wells," Journal of Vacuum Science & Technology B **18**(3), 1496-1501 (2000).

[3] Xin, Y. C., Li, Y., Martinez, A., Rotter, T. J., Su, H., Zhang, L., Gray, A. L., Luong, S., Sun, K., Zou, Z., Zilko, J., Varangis, P. M., and Lester, L. F., "Optical gain and absorption of quantum dots measured using an alternative segmented contact method," IEEE Journal of Quantum Electronics **42**(7), 725-732 (2006).

[4] K. Y. Lau and J. Paslaski, "Condition for short pulse generation in ultrahigh frequency mode-locking of semiconductor lasers", IEEE Photon. Tech. Lett., **3**, 974-976, (1991).

[5] C.-Y. Lin, Y.-C. Xin, Y. Li, F. L. Chiragh and L. F. Lester, "Cavity design and characteristics of monolithic long-wavelength InAs/InP quantum dash passively mode-locked lasers", Opt. Express, **17** 19739, (2009).

[6] M. T. Crowley, D. Murrell, N. Patel, M. Breivik, C.-Y. Lin, Y. Li, B.-O. Fimland and L. F. Lester, "Analytical Modeling of the Temperature Performance of Monolithic Passively Mode-Locked Quantum Dot Lasers" IEEE J. Quantum Electron. **18**, 1059, (2011).

[7] N. G. Usechak, Y.-C. Xin, C.-Y. Lin, L. F. Lester, D. J. Kane, and V. Kovanis, "Modeling and direct electric field measurements of passively mode-locked quantum-dot lasers," IEEE J. Sel. Top. Quantum Electron. **15**, 653–660 (2009).

[8] A. G. Vladimirov, and D. Turaev, "Model for passive mode locking in semiconductor lasers," Phys. Rev. A, **72**(3), 033808 (2005).

[9] G. Fiol, C. Meuer, H. Schmeckebier, D. Arsenijevic, S. Liebich, M. Laemmlin, M. Kuntz, and D. Bimberg, "Quantum-Dot Semiconductor Mode-Locked Lasers and Amplifiers at 40 GHz", IEEE J. Quantum Electron., 45, 1429-1435, (2009).

[10] M. A. Cataluna, D. B. Malins, A. Gomez-Iglesias, W. Sibbett, A. Miller, and E. U. Rafailov, "Temperature dependence of electroabsorption dynamics in an InAs quantum-dot saturable absorber at 1.3 μm and its impact on mode-locked quantum-dot lasers", Appl. Phys. Lett., **97**, 121110, (2010).

DEPARTMENT OF DEFENSE

DEFENSE THREAT REDUCTION
AGENCY
8725 JOHN J. KINGMAN ROAD
STOP 6201
FORT BELVOIR, VA 22060
ATTN: J. REED

DEFENSE TECHNICAL
INFORMATION CENTER
8725 JOHN J. KINGMAN ROAD,
SUITE 0944
FT. BELVOIR, VA 22060-6201
ATTN: DTIC/OCA

DEPARTMENT OF DEFENSE
CONTRACTORS

EXELIS, INC.
1680 TEXAS STREET, SE
KIRTLAND AFB, NM 87117-5669
ATTN: DTRIAC